Electrochimica Acta 213 (2016) 174–185

Contents lists available at ScienceDirect

Electrochimica Acta

journal homepage: www.elsevier.com/locate/electacta

Numerical and Experimental Investigation of Performance Characteristics of Lithium/Sulfur Cells

Kisoo Yoo[a], Min-Kyu Song[a], Elton J. Cairns[b,c], Prashanta Dutta[a,*]

[a] School of Mechanical and Materials Engineering, Washington State University, Pullman, United States
[b] Department of Chemical and Biomolecular Engineering, University of California, Berkeley, United States
[c] Environmental Energy Technologies Division, Lawrence Berkeley National Laboratory, United States

ARTICLE INFO

Article history:
Received 12 May 2016
Received in revised form 4 July 2016
Accepted 19 July 2016
Available online 20 July 2016

Keywords:
Li/S cell
Polysulfide solubility
Polysulfide shuttling
Overcharge

ABSTRACT

In this study, we propose a modified mathematical model for Lithium/Sulfur (Li/S) cells and present a detailed numerical analysis showing the effects of (1) the presence of solid sulfur species ($S_{8(s)}$, $Li_2S_{2(s)}$, $Li_2S_{(s)}$), (2) the solubility and diffusivity of polysulfides in the electrolyte, and (3) reaction rate constants of polysulfide reduction reactions at Li electrode on the electrochemical performance characteristics of Li/S cells including the cycling performance. The cell potential profiles predicted from numerical analysis were compared with experimental discharge and charge curves with emphasis on the possibility of the presence of the intermediate solid phase $Li_2S_{2(s)}$. Numerical results suggest that the cell potential obtained without the consideration of the intermediate solid phase $Li_2S_{2(s)}$ is in the best agreement with experimental results. Also, the polysulfide shuttling phenomenon has been numerically analyzed with electrolytes of different polysulfide solubility and compared with experimental cell discharge and charge curves. Our model clearly shows that the electrolyte of high polysulfide solubility and unprotected negative (anode) electrode can lead to unwanted reduction reactions of high-order polysulfides on the Li electrode, resulting in a significant overcharge problem. This agrees well with our experimental results for identical experimental conditions. Furthermore, the cycling performance of a Li/S cell was predicted, including the effect of the polysulfide shuttle on the subsequent discharge/charge curves. In the simulation, it was found that the high voltage plateau is reduced markedly in the discharge process after incomplete charge because sulfur (S_8) could not be recovered when the polysulfide shuttle problem is significant. Also, it is suggested that cycling performance of Li/S cells would be improved by limiting both the polysulfide diffusivity and the reduction reaction rate of high-order polysulfides at Li electrode during charge.

1. Introduction

Current lithium-ion (Li-ion) cells are approaching to their maximum specific energy (~200 Wh/kg at the cell-level) and are unable to provide sufficient energy storage capability for emerging technologies such as electric vehicles. Lithium/Sulfur (Li/S) cells can offer significantly greater practical (obtainable) specific energies (~600 Wh/kg), and can potentially lead to transformative changes in battery technology and replace current Li-ion cells [1,2]. In addition to the high theoretical specific energy, Li/S cells have several other advantages. For instance, one of the primary constituents of the cell, sulfur, is inexpensive, abundant on earth and environmentally benign. However, the successful development of Li/S cells as a commercial product has been hindered by the poor cycling performance of these cells, caused largely by the dissolution of sulfur (loss as polysulfides) and movement of these polysulfide species back and forth between anode and cathode in commonly used liquid electrolytes. Therefore, one of the biggest challenges is the selection of an appropriate electrolyte that allows good cyclability and high specific energy without compromising on safety standards. In order to address this challenge, it is essential to unveil the reaction mechanisms such as reduction/oxidation reactions and their pathways on the active material as well as precipitation and dissolution phenomena of solid phases in the Li/S cell.

Extensive experimental studies have been carried out to elucidate the electrochemical reaction process during the operation of Li/S cells. Nelson et al. [3] used *in-operando* x-ray diffraction

* Corresponding author.
E-mail address: prashanta@wsu.edu (P. Dutta).

http://dx.doi.org/10.1016/j.electacta.2016.07.110
0013-4686/

Nomenclature

Symbol	Description (Unit)
a	Specific surface area of cathode (m^2/m^3)
C_i	Concentration of species i ($mole/m^3$)
$C_{i,ref}$	Reference concentration of species i ($mole/m^3$)
$C_{i,ave}$	Average concentration of species i in cathode ($mole/m^3$)
D_i	Diffusivity of species i (m^2/s)
F	Faraday constant (C/mole)
i_i	Current density due to reaction i (A/m^2)
i_0^{ref}	Exchange current density of electrochemical reaction (A/m^2)
i_{load}	Load current density (A/m^2)
K_k	Solubility parameter of precipitate k ($mole/m^3$ (for $S_{8(l)}$) $mole^3/m^9$ (for $Li_2S_{(s)}$ and $Li_2S_{2(s)}$))
$k_{k,l}$	Rate constant of precipitate k (1/sec (for $S_{8(l)}$) m^6/mol^2-sec (for $Li_2S_{(s)}$ and $Li_2S_{2(s)}$))
k_{ps}	Reaction rate constant of high-order polysulfides reduction on Li anode (1/sec)
N_i	Flux of species i ($mole/m^2$-sec)
R	Gas constant (J/mole-K)
T	Temperature (K)
t	Time (sec)
V_k	Molar volume of the precipitate k (m^3/mole)
z_i	Charge number of species i
α	Symmetry coefficient
ε	Porosity of material
ε_k	Volume fraction of precipitate k
ϕ_l	Liquid phase electric potential (V)
ϕ_s	Solid phase electric potential (V)
η_i	Surface overpotential for electrochemical reaction i (V)
λ	ionic conductivity (S/m)
σ	Electric conductivity (S/m)

(XRD) to show structural and morphological changes as well as to identify polysulfide species involved in the electrochemical reactions of Li/S cells. Cuisinier et al. [4] used *in-operando* x-ray absorption spectroscopy (XAS) to study the mechanisms of sulfur redox chemistry during cycling, which showed how the sulfur fraction and sulfide precipitation impact capacity. However, those studies had the difficulty of identifying all polysulfide species during cell operation due to the limited resolution of *in-operando* XAS. Kawase et al. [5] analytically studied the electrochemical reaction process occurring within the cell using an organic conversion technique. In that work, *ex-situ* liquid chromatography-mass spectrometry (LC/MS) analysis was used to identify polysulfide species. Even though these studies clarified which polysulfide species are involved at certain discharge-charge depth, the precipitation/dissolution phenomena of lithium-polysulfides remain unclear.

A numerical analysis can be used to identify all reactant and product species involved in cell reactions during the discharge-charge process, including lithium ions, polysulfide ions and solid phase sulfur species. Therefore, one can investigate precisely the electrochemical behavior of a Li/S cell by performing numerical analysis based on a rigorous model. Kumaresan et al. [6] originally proposed a mathematical model for a Li/S cell to study the discharge process. Recently, Ghaznavi [7–9] expanded the model for sensitivity analysis by varying key parameters. However, those studies cannot be used to predict cycling performance of the cell since the model is missing an important reduction reaction of the high-order polysulfides (S_n^{2-}, $n \geq 4$) on Li electrode, which results in overcharge [10] and the polysulfide shuttling [11,12] problem. Earlier, Mikhaylik and Akridge [13] proposed a model describing reduction reactions of high-order polysulfides on Li electrode and discussed the shuttling problem, but their model did not include ion transport phenomena which would introduce concentration polarization. Recently, a mechanistic model including ion transportation was proposed by Hofmann et al. [14] to show the polysulfide shuttle and capacity loss in Li/S cells. However, the relation between polysulfide solubility and the shuttle problem is still unclear. Furthermore, the existence of the $Li_2S_{2(s)}$ phase near the end of the discharge process has been debated. For instance, *in-operando* XRD showed no formation of crystalline Li_2S [3], which contradicts *ex-situ* studies previously reported [15–17], while other *in-situ* studies indicated $Li_2S_{(s)}$ as a final stage crystalline lithium sulfide [4,18].

Therefore, in this work, we propose a modified mathematical model based on the work of Kumaresan et al. [6] and compare numerical results with experimental data to identify the ionic and solid phase species that are mainly involved in the electrochemical reactions in the Li/S cell. We use the experimentally validated numerical model to explain the roles of solid phase sulfur species for the electrochemical performance behavior of the Li/S cell. Moreover, the reduction reaction at the negative electrode during charge is modeled, and charging behavior is studied to reveal the polysulfide shuttling phenomenon leading to incomplete charge. Lastly, the cycling performances of the Li/S cell is analyzed with emphasis on the solubility and diffusivity of polysulfides and compared with experimental results of Li/S cells constructed with and without $LiNO_3$ additive in the electrolyte.

2. Theory

2.1. Chemical Reactions

In this section, we briefly review the general chemical reactions for a Li/S cell. A Li/S cell consists of a lithium anode (negative electrode) and a sulfur-carbon cathode (positive electrode) as a starting configuration. Upon discharging, at the anode side, lithium oxidizes to form lithium ions in the electrolyte that moves to the cathode material through the separator/electrolyte, while at the cathode side sulfur is reduced first to higher-order polysulfides, and then to lower order polysulfides and, eventually, lithium ions and lower-order polysulfides react to produce lithium sulfide ($Li_2S_{2(s)}$ and/or $Li_2S_{(s)}$) during the discharge process and the reverse occurs during charge.

Fig. 1 shows the schematic structure of a Li/S cell and details the chemical reactions involved. Here, ions and solvated species involved in the electrochemical reactions are specified as Li^+, S_n^{2-} ($n = 1, 2, 4, 6, 8$) and $S_{8(l)}$. Chemical reactions for these species are described by the Butler-Volmer equation and will be discussed in the mathematical model section. Other components, such as $S_{8(s)}$, $Li_2S_{2(s)}$ and $Li_2S_{(s)}$ are regarded as possible solid phases and a precipitation/dissolution model is applied only for them. The oxidation (during discharge) and reduction (during charge) reactions of polysulfides can also occur at Li electrode since polysulfide dissolves into the electrolyte and diffuses to the Li electrode side. However, the reduction reaction (e.g.: $S_{8(l)} \longrightarrow S_8^{2-}$) is considered at the negative electrode side during only the charge process, since the reduction of high-order polysulfides on the Li anode is only significant during the charging process [10,19].

2.2. Modified Mathematical Model

Although Kumaresan et al. [6] have presented the basic mathematical model for the Li/S cell, their proposed model is

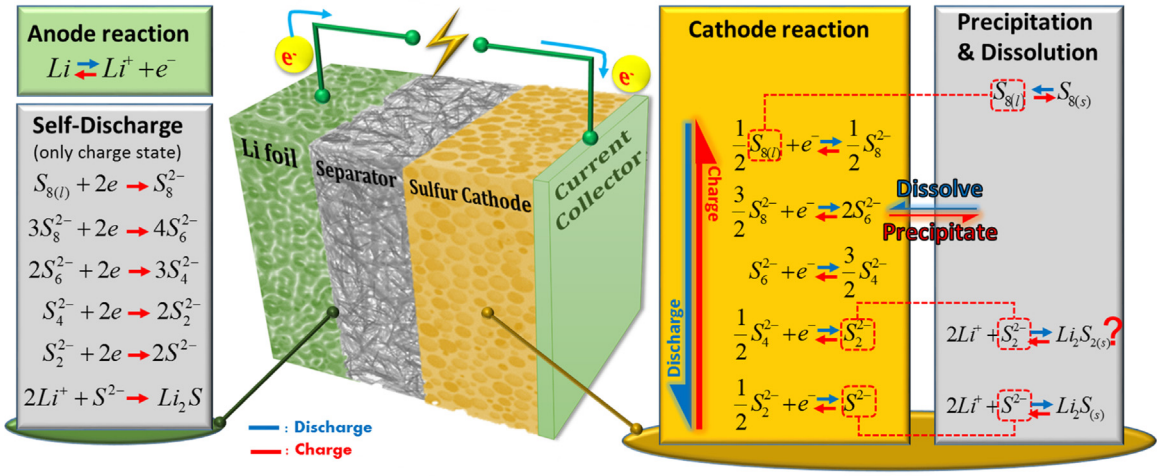

Fig. 1. Schematic of a Li/S cell showing various components and possible chemical reactions at the anode (negative electrode) and cathode (positive electrode) side. Phase change (both dissolution and precipitation) occurs at the positive electrode during charge and discharge. The discharge process is shown by the blue arrow, while the charge process is denoted by the red arrow. (For interpretation of the references to colour in this figure legend, the reader is referred to the web version of this article.)

numerically unstable for high solubility of lithium polysulfides. For instance, the volume fractions (ε) of $Li_2S_{2(s)}$ and $Li_2S_{(s)}$ could approach zero during the calculations of higher-potential discharge due to the higher solubility of lithium polysulfides. Once the volume fraction becomes zero, the precipitation to $Li_2S_{2(s)}$ and $Li_2S_{(s)}$ cannot occur in the positive electrode side during discharge even if the concentration of S_2^{2-} or S^{2-} is over the solubility limit. Also, the volume fraction of $S_{8(s)}$ can suffer from the same numerical instability during the charge process. Thus, to circumvent the undesired numerical issue, the precipitation and dissolution model is modified in our numerical scheme by adding an extra term as

$$\frac{\partial \varepsilon_{S_{8(s)}}}{\partial t} = V_{S_{8(s)}}\left[k_{S_{8(s)},1}\varepsilon_{S_{8(s)}}\left(C_{S_{8(l)}} - K_{S_{8(l)}}\right) + k_{S_{8(s)},2}\frac{C_{S_{8(l)}}}{\varepsilon_{S_{8(s)}}}\right] \quad (1-\text{a})$$

$$\frac{\partial \varepsilon_{Li_2S_{2(s)}}}{\partial t} = V_{Li_2S_{2(s)}}\left[k_{Li_2S_2,1}\varepsilon_{Li_2S_{2(s)}}\left(C_{Li^+}^2 C_{S_2^{2-}} - K_{S_2^{2-}}\right) + k_{Li_2S_2,2}\frac{C_{Li^+}^2 C_{S_2^{2-}}}{\varepsilon_{Li_2S_{2(s)}}}\right] \quad (1-\text{b})$$

$$\frac{\partial \varepsilon_{Li_2S_{(s)}}}{\partial t} = V_{Li_2S_{(s)}}\left[k_{Li_2S,1}\varepsilon_{Li_2S_{(s)}}\left(C_{Li^+}^2 C_{S^{2-}} - K_{S^{2-}}\right) + k_{Li_2S,2}\frac{C_{Li^+}^2 C_{S^{2-}}}{\varepsilon_{Li_2S_{(s)}}}\right] \quad (1-\text{c})$$

where V, k and K are molar volume, precipitation/dissolution rate constant, and solubility parameter, respectively. In these equations, the additional term is only effective if the value of the volume fraction is very small.

Moreover, in our study, a reduction reaction of high-order polysulfides at the negative electrode is added to investigate the polysulfide shuttling problem. The rate of the high-order polysulfide reduction reaction at the negative electrode surface is directly related to the concentration of high-order solvated polysulfides as

$$\frac{dC_{S_{8(l)}}}{dt} = -\left(k_{ps1}C_{S_{8(l)}}\right) \quad (2-\text{a})$$

$$\frac{dC_{S_8^{2-}}}{dt} = \left(-k_{ps2}C_{S_8^{2-}} + k_{ps1}C_{S_{8(l)}}\right) \quad (2-\text{b})$$

$$\frac{dC_{S_6^{2-}}}{dt} = \left(-k_{ps3}C_{S_6^{2-}} + \frac{4}{3}k_{ps2}C_{S_8^{2-}}\right) \quad (2-\text{c})$$

$$\frac{dC_{S_4^{2-}}}{dt} = \left(-k_{ps4}C_{S_4^{2-}} + \frac{3}{2}k_{ps3}C_{S_6^{2-}}\right) \quad (2-\text{d})$$

$$\frac{dC_{S_2^{2-}}}{dt} = \left(-k_{ps5}C_{S_2^{2-}} + 2k_{ps4}C_{S_4^{2-}}\right) \quad (2-\text{e})$$

where k_{ps} is the reaction rate constant of high-order polysulfides reduction. As mentioned in the previous section, it is assumed that the high-order polysulfides reduction reaction at Li electrode occurs during the charge process only. All other governing equations and boundary conditions are introduced in Tables 1 and 2, respectively.

2.3. Computational Method

2.3.1. Assumptions

Dendrite formation and sulfur agglomeration are not considered in this macroscopic model. Thus, a one-dimensional analysis is sufficient to show the battery performance. Other assumptions used in this study are

1. Metallic type lithium foil is used as anode material so that porous separator and cathode are only considered as computational domain.
2. Species concentration gradient is dominant from anode to cathode (or cathode to anode) since the species transport occurs mainly in that direction.
3. Effect of EDL (electrode double layer), SEI (solid-electrolyte interface) and dendrite formation are negligible for capturing macroscopic phenomena.

Table 1
Chemical reactions at the anode and cathode, and mathematical models for species concentrations and electric potentials. Properties and constant values are same as reported in [6].

Anode reaction	$Li \leftrightarrow Li^+ + e^-$	$i_1 = i_1^{ref}\left[\exp\left(\frac{\alpha F}{RT}\eta_1\right) - \exp\left(-\frac{(1-\alpha)F}{RT}\eta_1\right)\right]$
Cathode reaction	$\frac{1}{2}S_{8(l)} + e^- \leftrightarrow \frac{1}{2}S_8^{2-}$	$i_2 = i_2^{ref}\left[\left(\frac{C_{S_8^{2-}}}{C_{S_8^{2-}}^{ref}}\right)^{0.5}\exp\left(\frac{\alpha F}{RT}\eta_2\right) - \left(\frac{C_{S_{8(l)}}}{C_{S_{8(l)}}^{ref}}\right)^{0.5}\exp\left(-\frac{(1-\alpha)F}{RT}\eta_2\right)\right]$
	$\frac{3}{2}S_8^{2-} + e^- \leftrightarrow 2S_6^{2-}$	$i_3 = i_3^{ref}\left[\left(\frac{C_{S_6^{2-}}}{C_{S_6^{2-}}^{ref}}\right)^{2}\exp\left(\frac{\alpha F}{RT}\eta_3\right) - \left(\frac{C_{S_8^{2-}}}{C_{S_8^{2-}}^{ref}}\right)^{1.5}\exp\left(-\frac{(1-\alpha)F}{RT}\eta_3\right)\right]$
	$S_6^{2-} + e^- \leftrightarrow \frac{3}{2}S_4^{2-}$	$i_4 = i_4^{ref}\left[\left(\frac{C_{S_4^{2-}}}{C_{S_4^{2-}}^{ref}}\right)^{1.5}\exp\left(\frac{\alpha F}{RT}\eta_4\right) - \left(\frac{C_{S_6^{2-}}}{C_{S_6^{2-}}^{ref}}\right)\exp\left(-\frac{(1-\alpha)F}{RT}\eta_4\right)\right]$
	$\frac{1}{2}S_4^{2-} + e^- \leftrightarrow S_2^{2-}$	$i_5 = i_5^{ref}\left[\left(\frac{C_{S_2^{2-}}}{C_{S_2^{2-}}^{ref}}\right)\exp\left(\frac{\alpha F}{RT}\eta_5\right) - \left(\frac{C_{S_4^{2-}}}{C_{S_4^{2-}}^{ref}}\right)^{0.5}\exp\left(-\frac{(1-\alpha)F}{RT}\eta_5\right)\right]$
	$\frac{3}{2}S_2^{2-} + e^- \leftrightarrow S^{2-}$	$i_6 = i_6^{ref}\left[\left(\frac{C_{S^{2-}}}{C_{S^{2-}}^{ref}}\right)\exp\left(\frac{\alpha F}{RT}\eta_6\right) - \left(\frac{C_{S_2^{2-}}}{C_{S_2^{2-}}^{ref}}\right)^{0.5}\exp\left(-\frac{(1-\alpha)F}{RT}\eta_6\right)\right]$
Ion concentration (mass transport)	$\frac{\partial(\varepsilon C_i)}{\partial t} = \nabla\cdot\left(\varepsilon^{1.5}D_i\nabla C_i\right) + z_i\omega_i\varepsilon C_i\nabla\phi_l + S_i$ where i = $\{Li^+, S_{8(l)}, S_8^{2-}, S_6^{2-}, S_4^{2-}, S_2^{2-}, S^{2-}\}$	
	$S_{Li^+} = -2\left[\frac{1}{V_{Li_2S_{8(s)}}}\frac{\partial\varepsilon_{Li_2S_{8(s)}}}{\partial t} + \frac{1}{V_{Li_2S_{6(s)}}}\frac{\partial\varepsilon_{Li_2S_{6(s)}}}{\partial t} + \frac{1}{V_{Li_2S_{4(s)}}}\frac{\partial\varepsilon_{Li_2S_{4(s)}}}{\partial t} + \frac{1}{V_{Li_2S_{2(s)}}}\frac{\partial\varepsilon_{Li_2S_{2(s)}}}{\partial t} + \frac{1}{V_{Li_2S_{(s)}}}\frac{\partial\varepsilon_{Li_2S_{(s)}}}{\partial t}\right]$	
	$S_{S_{8(l)}} = \frac{a}{F}(0.5i_2) - \frac{1}{V_{S_{8(s)}}}\frac{\partial\varepsilon_{S_{8(s)}}}{\partial t}$	
	$S_{S_8^{2-}} = \frac{a}{F}(-0.5i_2 + 1.5i_3)$	
	$S_{S_6^{2-}} = \frac{a}{F}(-2i_3 + i_4)$	
	$S_{S_4^{2-}} = \frac{a}{F}(-1.5i_4 + 0.5i_5)$	
	$S_{S_2^{2-}} = \frac{a}{F}(-i_5 + 0.5i_6) - \frac{1}{V_{Li_2S_{2(s)}}}\frac{\partial\varepsilon_{Li_2S_{2(s)}}}{\partial t}$	
	$S_{S^{2-}} = \frac{a}{F}(-i_6) - \frac{1}{V_{Li_2S_{(s)}}}\frac{\partial\varepsilon_{Li_2S_{(s)}}}{\partial t}$	
Electric potential in electrolyte	$\nabla\cdot\left(\varepsilon^{1.5}\lambda\nabla\phi_l\right) = -\nabla\cdot\left[F\sum\left(z_i\varepsilon^{1.5}D_i\nabla C_i\right)\right] - a(i_2 + i_3 + i_4 + i_5 + i_6)$ where λ is ionic conductivity	
Electric potential in cathode	$\nabla\cdot\left[(1-\varepsilon)^{1.5}\sigma\nabla\phi_s\right] = a(i_2 + i_3 + i_4 + i_5 + i_6)$ where σ is electric conductivity	

4. The high-order polysulfide reduction reactions at Li electrode occur during the charge process only.
5. Diffusion correlation between each species is weak so that self-diffusion coefficient is used for species transport equations.

2.3.2. Numerical Scheme

We used a finite volume method to construct linear algebraic equations for numerical modeling of the Li/S cell [20,21]. Discretized algebraic equations were obtained using a power law scheme for both mass conservation and charge conservation equations. Time dependent equations were solved by an implicit method for numerical stability. The Thomas algorithm was used to solve the tri-diagonal system of linear algebraic equations. The tolerances for the mass and charge conservation equations are 10^{-5}. Numerical simulations were performed on an Intel Xeon 2.2 GHz CPU.

3. Experimental Section

Sulfur-graphene oxide (S-GO) nanocomposite powders were synthesized using a method previously reported [1,22] and used as active material for the sulfur electrodes in this study. The sulfur electrodes were fabricated by mixing the S-GO nanocomposite, carbon black (Super C65) with a binder, polyvinylidene fluoride (PVDF), at a weight ratio of 70:20:10 in N-methyl-2-pyrrolidone (NMP) solvent to form slurry using an ultrasonicator. The resulting slurry was deposited on pure aluminum foil using a doctor blade (Elcometer 3540 Bird Film Applicator). After drying in a vacuum oven at 50 °C for 48 hours, the electrode was cut into circular pieces with a diameter of 12.7 mm for L/S cell assembly.

For the electrolyte, 1 M lithium bis(trifluoromethylsulfonyl) imide (LiTFSI, Sigma-Aldrich) in an organic solvent mixture of 1,3-dioxolane (DOL) and 1,2-dimethoxyethane (DME) mixture (1:1 by volume) was prepared and used for evaluation of the electrochemical performance of the Li/S cell with electrolytes of *high polysulfide solubility* [23]. For *electrolytes of low polysulfide*

Table 2
Boundary conditions for various governing equations presented in Table 1.

	Anode-Electrolyte	Separator-Cathode	Cathode-Current Corrector
Mass conservation	$N_{Li^+} = \frac{i_{load}}{F}$ $N_i = 0$ for other ions		$N_i = 0$
Electric potential in electrolyte	$\lambda\nabla\phi_l = -i_{load}$		$\nabla\phi_l = 0$
Electric potential in cathode		$\nabla\phi_s = 0$	$\sigma\nabla\phi_s = -i_{load}$

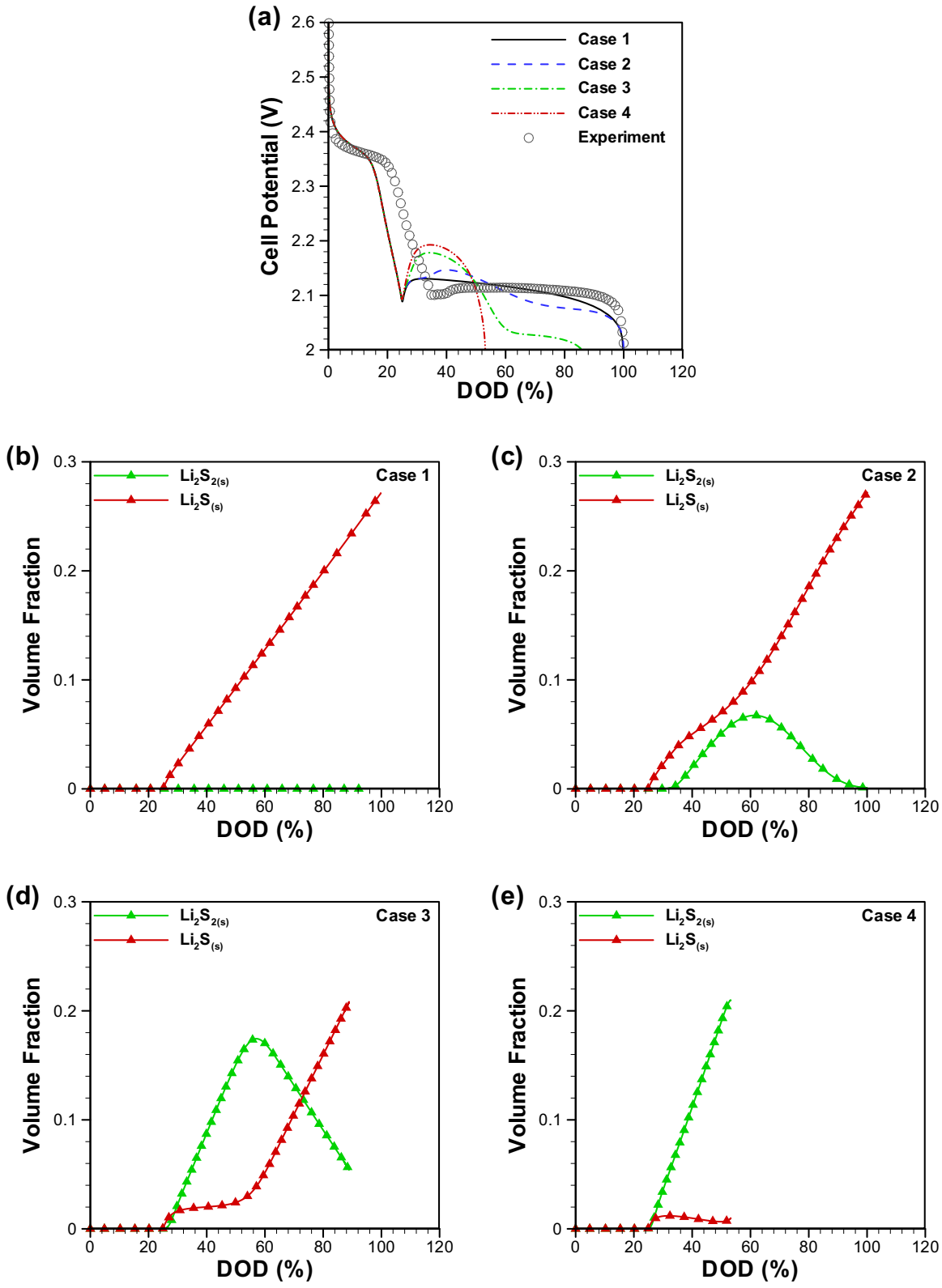

Fig. 2. (a) Numerically predicted and experimentally observed cell potential profiles during the discharge process for a current density of 0.1C. A hybrid electrolyte consisting of ionic liquid and organic solvent (1 M LiTFSI in PYR14TFSI/DOL/DME mixture (2:1:1 by volume)) was used as electrolyte in the experimental work. Four different cases are considered in the numerical study based on the different proportions of crystalline $Li_2S_{2(s)}$ and $Li_2S_{(S)}$. Numerically predicted volume fractions of crystalline $Li_2S_{2(s)}$ and $Li_2S_{(S)}$ for (b) case 1, (c) case 2, (d) case 3, and (e) case 4. Volume fraction values are averaged in the sulfur electrode region [6].

solubility, n-methyl-(n-butyl) pyrrolidinium bis(trifluoromethanesulfonyl)imide (PYR14TFSI, Sigma-Aldrich) was introduced to form 1 M LiTFSI in PYR14TFSI/DOL/DME mixture (2:1:1 by volume) as a pyrrolidinium-based ionic liquid. PYR14TFSI has been used successfully as an effective solvent to minimize the polysulfide shuttle with lower polysulfide solubility [24,25].

CR2032-type coin cells were assembled by sandwiching two separators (Celgard 2400) between a lithium metal foil (99.98%, Cyprus Foote Mineral) and a sulfur electrode fabricated with the S-GO composite in an argon-filled glove box. Constant-current discharge and charge testing of the coin cells were performed using a battery cycler (Maccor Series 4000) at a load current density of 0.1C (1C = 1675 mA/g) between 1.7 and 2.8 V. The cell capacity was normalized by the weight of sulfur. All electrochemical characterizations were conducted inside a temperature chamber (TestEquity TEC1) controlled at 30 °C.

4. Results and Discussion

4.1. Discharge and Charge Characteristics

In a Li/S cell, it has been reported that two plateaus appear in the cell potential profile during the discharge process. The first (high voltage) plateau requires constant concentration of $S_{8(l)}$ for production of S_8^{2-}, which is the significant reduction reaction. The constant concentration of $S_{8(l)}$ can be maintained if $S_{8(s)}$ can be continuously dissolved into the electrolyte. On the other hand, the second plateau is due to the formation of solid lithium sulfides ($Li_2S_{2(s)}$ and/or $Li_2S_{(s)}$) while it is not clear which crystalline species is formed or dominant during the discharge process. For instance, Nelson et al. claimed "it was found that crystalline Li_2S does not form at the end of discharge for all sulfur cathodes studied" [3], but Cuisinier et al. reported crystalline Li_2S as the discharge product at the end of discharge [4]. On the other hand, Manthiram et al. suggested $Li_2S_{2(s)}$ and $Li_2S_{(s)}$ as the final discharge product [26]. Therefore, in this study, we investigated the cell potential profiles depending on the relative presence of solid product species $Li_2S_{2(s)}$ and $Li_2S_{(s)}$ to show the possible final solid phase in a Li/S cell. The numerical simulation has been carried out for four different conditions. In Case 1, it was hypothesized that crystalline $Li_2S_{2(s)}$ rarely forms, while, in Case 4, the crystalline Li_2S_2 formation is significant. Case 2 and Case 3 assumed that the crystalline formation of Li_2S_2 is more than Case 1 and less than Case 4, respectively.

Fig. 2(a) shows the cell potential profiles for each case. It is notable that, for the all cases, a small valley appears at near the 30% depth of discharge (DOD), in which precipitation started. The precipitation reaction mitigates supersaturation of polysulfide (S_2^{2-} and S^{2-}) [6] and it alleviates a potential drop due to concentration polarization. After this singular point (over 30% DOD), each case produces a different cell potential profile. In Case 1, the simulation shows the most linear cell potential profile and full discharge depth is obtained. Here, specific capacity at 100% DOD is 1675 mAh/g and the value is the same as the theoretical specific capacity which can be achieved in a Li/S cell. However, the cell potential profiles were distorted in Cases 2 and 3 and, eventually, the cell potential sharply dropped before reaching full discharge in Case 4. In Cases 2 and 3, a higher cell potential appears in the 30 ~ 55% DOD region since supersaturated S_2^{2-} precipitates to $Li_2S_{2(s)}$, (see Fig. 2(c) and (d)), and it alleviates the potential loss due to concentration polarization. However, the cell potential drops to a lower value after dissolution of $Li_2S_{2(s)}$ starts (over 55% DOD). Here, the lower potential is obtained due to the kinetic resistance of the solid phase change, $Li_2S_{2(s)} \rightarrow Li_2S_{(s)}$ (see Fig. 2(c) and (d)). For Case 4, the precipitation of $Li_2S_{2(s)}$ is significant and mostly due to S_2^{2-} ions, reduced from high-order polysulfide, precipitating to $Li_2S_{2(s)}$ (see Fig. 2(e)). For this case, the discharge potential suddenly drops at 55% DOD when the fraction of $Li_2S_{2(s)}$ reaches its maximum value. At this stage, the discharge reaction solely depends on the solid-state phase change reaction ($Li_2S_{(s)} \rightarrow Li_2S_{(s)}$) and this solid state reaction introduces large kinetic resistance, resulting in a massive potential drop [27,28].

As shown in Fig. 2 (a), the cell potential profile significantly varies with the presence of $Li_2S_{2(s)}$ and, by comparing cell potential profiles between numerical analysis and experimental results, it can be suggested which model (presence or absence of $Li_2S_{2(s)}$) can properly predict the Li/S cell performance during the discharge process. In Fig. 2 (a), the circle symbols show the cell potential profile obtained experimentally. The experimental profile clearly demonstrates the appearance of two plateaus and especially, distortion of the second plateau cannot be seen. Here, the cell potential profile obtained from the numerical analysis for Case 1 is the only model in good agreement with the experimental results. Hence, the absence of $Li_2S_{2(s)}$ during the discharge process (Case 1) is considered as the most reasonable model for this system.

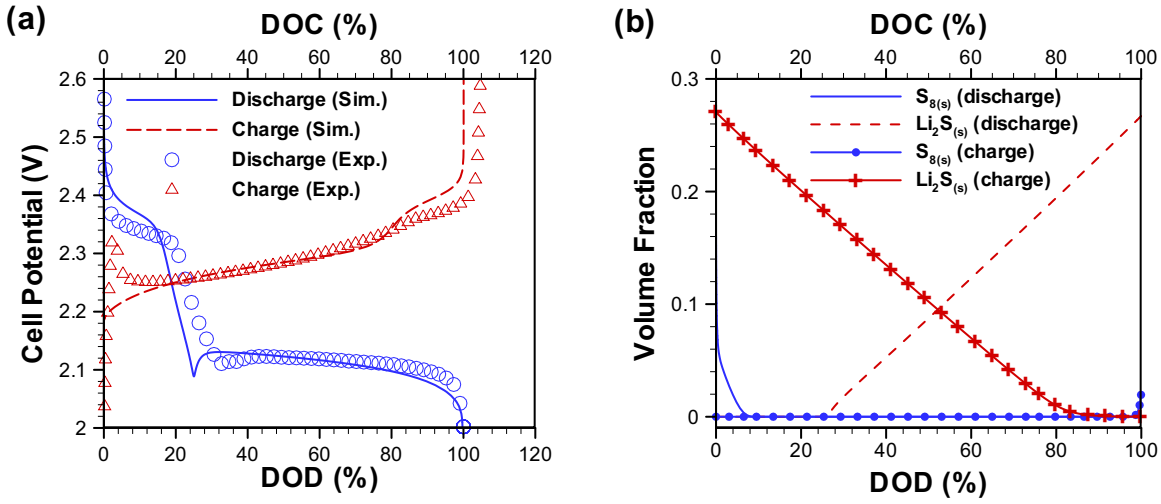

Fig. 3. (a) Numerical and experimental cell potential profiles during the discharge and charge processes for a current density of 0.1C. A hybrid electrolyte consisting of ionic liquid and organic solvent (1 M LiTFSI in PYR14TFSI/DOL/DME mixture (2:1:1 by volume)) was used in the experimental study. (b) Volume fractions of crystalline $S_{8(s)}$ and $Li_2S_{(s)}$ during the discharge and charge processes.

Moreover, there are several references [4,29] to support this assumption. Referring to the comparison between numerical and experimental results as well as the literature, we modified the mathematical model by considering $S_{8(s)}$ and $Li_2S_{(s)}$ as the only possible solid species in the Li/S cell and, used this modified model in the rest of this paper.

In addition to the cell performance during discharge, the cell potentials are calculated at different depths of charge (DOC) and compared with the experimental results (Fig. 3). Similar to the discharge process, the cell potential strongly depends on the dissolution of $Li_2S_{(s)}$ and precipitation of crystalline $S_{8(s)}$. The charge potential gradually increases with DOC as shown in Fig. 3(a). As aforementioned in the analysis of the discharging process, the concentration of reactant (S^{2-}) has been maintained in $0 \sim 80\%$ for the DOC region during the charge process because of the continuous dissolution of $Li_2S_{(s)}$. Therefore, the potential drop due to concentration polarization is insignificant at this stage. However, once $Li_2S_{(s)}$ is completely dissolved and depleted (see Fig. 3(a) and (b), at 80% DOC), the charge potential increases more due to the concentration polarization of the reactant. After that stage, the charge potential increase is slightly alleviated due to precipitation of $S_{8(s)}$, resulting in reduced $S_{8(l)}$ concentration, but, eventually, the potential soars sharply near the fully charged stage. Here, the predicted charge profile is compared with the experimental results. In Fig. 3 (a), delta symbols show the cell potential profile obtained from experiments during the charge process. In the beginning of the charging stage, a large potential barrier is observed. After the barrier, the charge potential increases gradually and it is elevated more near the 80% DOC. However, the potential increase is alleviated soon and, eventually, it soars near the fully charged state (100% DOC). Here, the potential barrier at the beginning of the charge process is due to the high electronic resistivity and low lithium ion diffusivity in $Li_2S_{(s)}$ [30]. In our continuum model, the microscopic mechanism is not involved and the simulation could not capture this potential barrier. However, except for the barrier, the experimental charge potential profile is in good agreement with our numerical results (see Fig. 3 (a)). By comparing the numerical and experimental results, we adequately validated the modified numerical model that can precisely elucidate the discharge and charge processes in Li/S cells.

4.2. Modeling of Overcharge Problem and Implications

In Li/S cells, the reduction reaction of high-order polysulfides at the negative electrode introduces polysulfide shuttling resulting in a cell overcharge problem. As mentioned in the chemical reaction section, during the charge process, $S_{8(l)}$, oxidized from S_8^{2-}, moves to the negative electrode and is reduced to S_8^{2-} (see Fig. 1). Similarly, S_8^{2-}, S_6^{2-} S_4^{2-} S_2^{2-} and S^{2-} can be reduced to low-order polysulfides and lithium sulfide. Therefore, the charging current is partly used to reduce high-order polysulfides at the negative electrode in addition to the regular oxidation reaction at the positive electrode for formation of polysulfides during charge process. This is commonly known as the overcharge problem. In this study, to reveal the overcharge phenomena in the Li/S cell, the charge behavior was investigated with two extreme cases. In the first case, polysulfide shuttling is set to be insignificant due to the low solubility of polysulfides and the slow reduction reaction for polysulfides at the negative electrode. In the other case, the shuttling can be significant because of high solubility and a fast reduction reaction.

Table 3
Values of parameters used for varying polysulfide solubility simulation.

Simulation conditions	Solubility parameters	
	$K_{S_{8(s)}}$	$K_{Li_2S_{(s)}}$
Low solubility of polysulfide	10 mole/m^3	10^4 mole^3/m^9
High solubility of polysulfide	190 mole/m^3	5×10^4 mole^3/m^9

Table 4
Reaction rate constants of high-order polysulfides reduction reactions.

Simulation Case	Reaction rate constant (1/sec)				
	k_{PS1}	k_{PS2}	k_{PS3}	k_{PS4}	k_{PS5}
Case-A	1×10^{-9}	1×10^{-12}	1×10^{-12}	5×10^{-12}	5×10^{-12}
Case-B	1×10^{-7}	1×10^{-12}	1×10^{-12}	5×10^{-12}	5×10^{-12}
Case-C	1×10^{-7}	1×10^{-8}	1×10^{-12}	5×10^{-12}	5×10^{-12}
Case-D	1×10^{-7}	1×10^{-8}	1×10^{-9}	5×10^{-12}	5×10^{-12}

Here, the solubility of polysulfides can be controlled with the values of the solubility parameter (K), with greater K values indicating higher solubility of polysulfides. The solubility parameter values that are used in the simulation for each case are shown in Table 3. Solubility parameters were calculated from maximum concentration of species that can be dissolved into an electrolyte. For example, $K_{S_{8(s)}}$ value is obtained directly from maximum concentration of dissolved S_8 in an electrolyte. The precipitation of solid S_8 occurs when concentration of $S_{8(l)}$ is higher than the solubility parameter value and vice versa for dissolution. Similarly, value for $K_{Li_2S_{(s)}}$ was obtained from maximum soluble concentration of Li_2S as $K_{Li_2S_{(s)}} = C_{Li,ini}{}^2 \cdot C_{Li_2S_{(s)},\max}$. Here $C_{Li,ini}$ is the initial concentration of lithium ion in the electrolyte.

The reduction reaction rate can be controlled with the reduction reaction rate constant (k_{PS}). For the low polysulfide solubility and slow reduction reaction (Case-A, Table 4), the Li/S cell could be fully charged as shown in Fig. 4(a). Here, the concentration of $S_{8(l)}$ is under 10 mole/m^3 as shown in Fig. 4(b) and S_8^{2-} is fully converted to $S_{8(l)}$ at the end of the charge (see Fig. 4(c)). At the same time, $S_{8(l)}$ is also precipitated as $S_{8(s)}$ and the volume fraction of $S_{8(s)}$ has approximately reached to its initial value as shown in Fig. 4(c). The polysulfide oxidation reaction happens progressively from S^{2-} to $S_{8(l)}$ and, eventually, $S_{8(s)}$ is fully recovered since the reduction reaction of polysulfides is weak at the negative electrode.

The numerically predicted cell performance characteristics are consistent with our experimental results. In Fig. 4(a), circle symbols show experimental cell potential for the Li/S cell using the electrolyte (1 M LiTFSI in P14TFSI/DOL/DME mixture) with $LiNO_3$ additive. In this case, the cell can be fully charged in the presence of $LiNO_3$ because the anode protection layer (APL) can be formed at Li electrode surface to block the reduction reaction by adding $LiNO_3$ to the electrolyte. Moreover, in this case, since the ionic liquid-based electrolyte which has low polysulfide solubility [31] is used as the electrolyte, the high-order polysulfide reduction reaction is insignificant so that the overcharge problem is rarely noticed. This result agrees well with our simulation results that use the condition of low polysulfide solubility and low reaction rate constant of high-order polysulfide reduction (see Fig. 4(a)).

In contrast, Fig. 5(a) shows numerical results with high solubility for polysulfides and considerable reduction reaction at the negative electrode surface. The reduction reaction constants for each polysulfide specified in Table 4 were used to study the reaction pathways resulting in incomplete charging. Serious overcharge problems are observed for all simulation cases. Constant charging potential was noted after a certain depth of charge stage, and the cell could not reach the cutoff voltage corresponding to the fully charge condition.

The constant charging potentials vary considerably in each case. For example, the charging value is limited at 2.35 V for the Case-B which illustrate that the reduction reaction of $S_{8(l)}$ is most

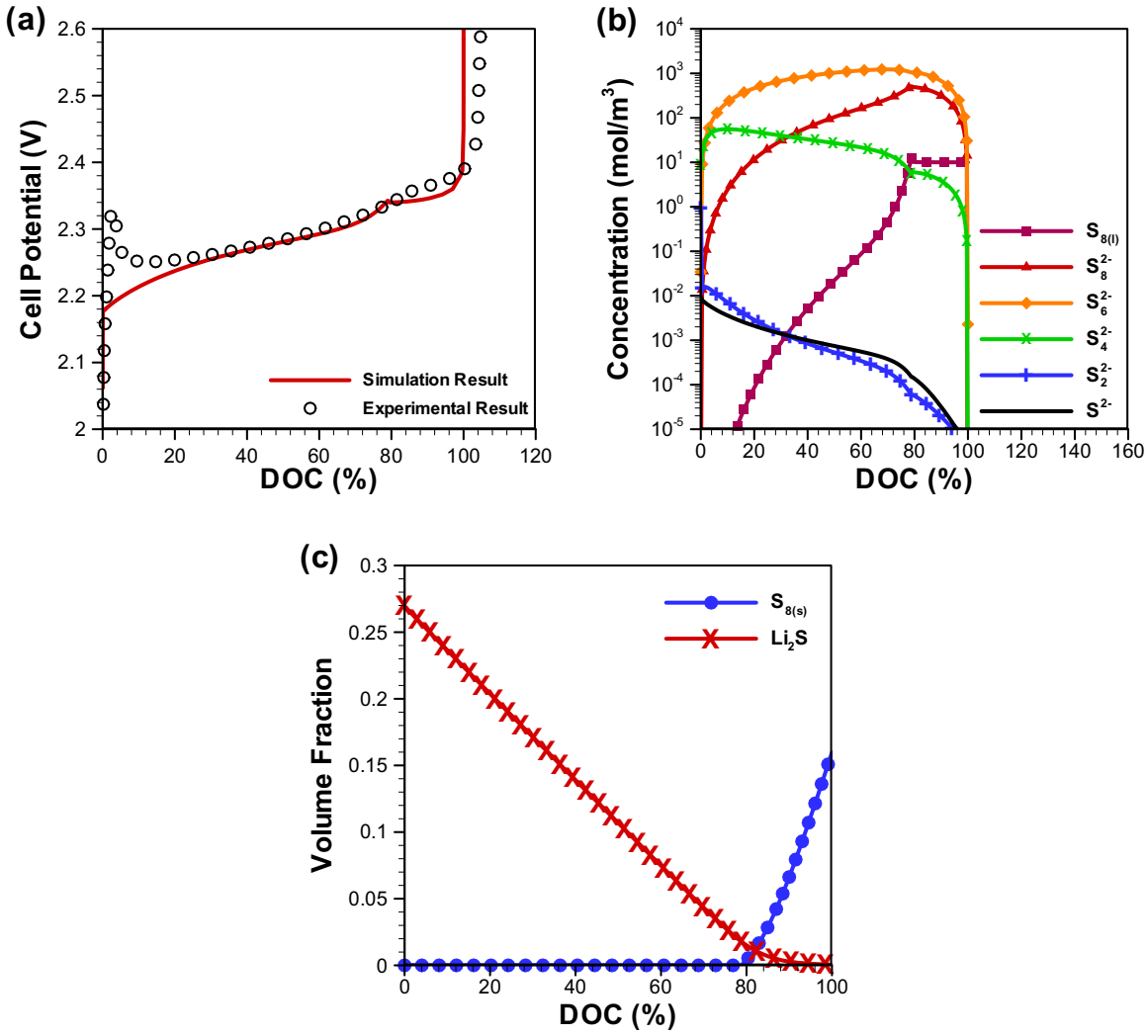

Fig. 4. (a) Numerical and experimental charge curves of the Li/S cell using electrolyte having low solubility for polysulfides with low reaction rate constant of high-order polysulfides reduction on the Li anode (Case-A). Electrolyte used in the experimental work is same as in Fig. 3. The reaction rate constants of high-order polysulfides are given in Table 4 (Case-A). (b) Numerically predicted (averaged) concentration of solvated phase polysulfides in the cathode region during the charge process for a Li/S cell modeled with an electrolyte having low solubility for polysulfides. (c) Numerically predicted volume fraction of crystalline $S_{8(s)}$ and $Li_2S_{(s)}$ during the charge process.

significant. Meanwhile, lower constant potentials, 2.32 V and 2.28 V, are observed for the Case-C and D, respectively. In Case-B, even though $S_{8(l)}$ can be recovered with oxidation reaction from S_8^{2-} at the positive electrode, the concentration of $S_{8(l)}$ is immediately reduced due to the formation of S_8^{2-} by the reduction reaction at the negative electrode at the same time (see Fig. 5(b)). Therefore, the charging potential is maintained at the reaction potential due to incomplete polysulfide recovery and infinitely long charging occurs. However, in Case C, it is more difficult to recover $S_{8(l)}$ from S_8^{2-} (see Fig. 5(c)) since most of the S_8^{2-} intensively reduces to S_6^{2-} at the negative electrode before S_8^{2-} oxidizes to $S_{8(l)}$ at the positive electrode. As a result of incomplete recovery, the charging potential is limited by the oxidation reaction of S_8^{2}. For case D, less $S_{8(l)}$ and S_8^{2-} are recovered than in Case B and C (see Fig. 5(d)), and the lower charging potential is observed.

Considering the charging behaviors, it is noteworthy that the charging potential significantly varies with the reduction reaction pathway at the negative electrode. Hence, we can find which specific reduction reaction at the negative electrode can lead to the infinite charging problem by comparing simulation and experimental cell potential profiles. For the comparison, the Li/S cell was tested with an inferior electrolyte and electrode, which are likely to induce a significant polysulfide shuttling problem. 1 M LiTFSI in DOL/DME without $LiNO_3$ was used as electrolyte with high solubility of polysulfides because the organic electrolyte has a high solubility for polysulfide compared to ionic liquids. Furthermore, the polysulfide reduction reaction is significant at the negative electrode during charging because of the absence of the APL (no $LiNO_3$). In this experiment, the infinite charging problem was also observed (see Fig. 5(a) circle symbols). The experimental charging behavior of the cell follows the trend predicted by the model with a significant reduction reaction of S_6^{2-} (simulation Case-D). Therefore, we can attribute the overcharge problem to the significant reduction reaction at the negative electrode and high solubility of polysulfides in the electrolyte. The results also suggest that S_6^{2-} reduction mainly led to the infinite charging phenomenon in this system.

4.3. Prediction of Cycling Performance

Cycling performance is a key issue in Li/S cells. It is well known that Li/S cells suffer from short cycle lives due to the polysulfide shuttling. As mentioned in the previous section, the overcharge problem is significant when the high-order polysulfide reduction reaction on the Li electrode occurs intensively. Hence, in this section, cycling performance is predicted and investigated with

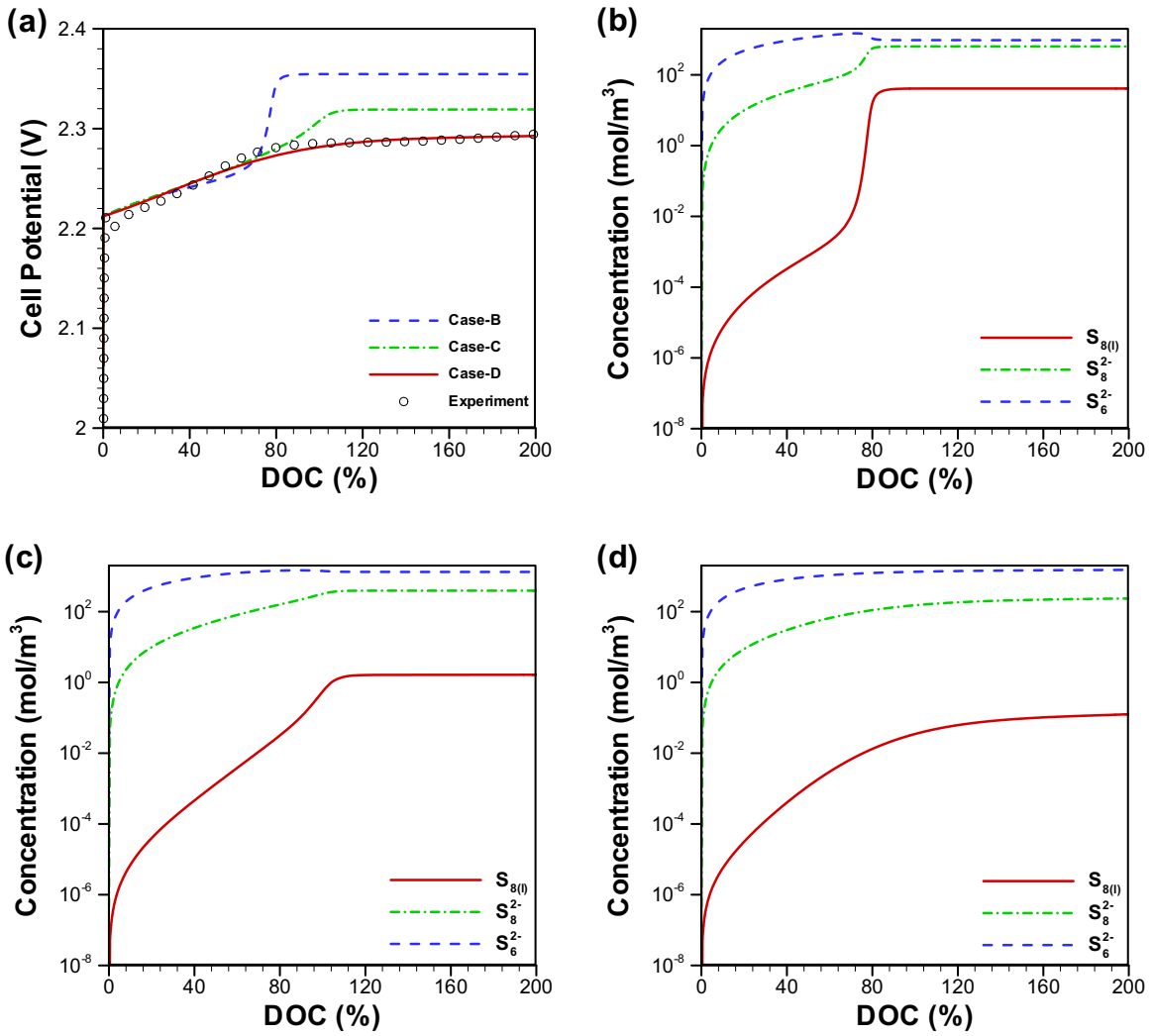

Fig. 5. (a) Numerical and experimental charge curves of a Li/S cell. An organic electrolyte with high polysulfide solubility (1 M LiTFSI in DOL/DME mixture (1:1 by volume)) was used in the experimental work. The reaction rate constants of high-order polysulfides are given in Table 4 for case- B, C and D. Numerically predicted (averaged) concentration of the solvated polysulfide for (b) Case-B (c) Case-C (d) Case-D in the cathode region during the charge process for a Li/S cell modeled using an electrolyte with high polysulfide solubility.

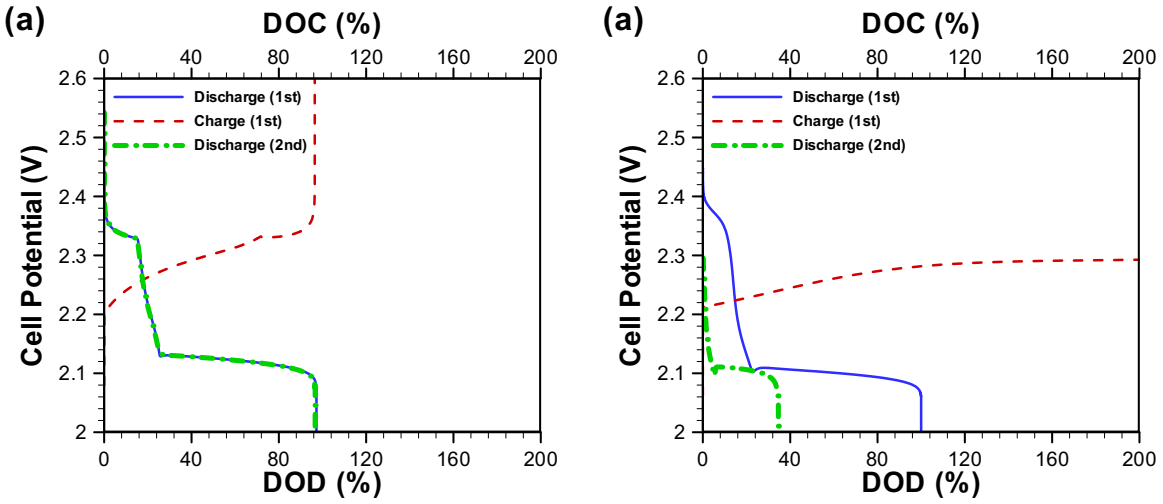

Fig. 6. Simulated cell potential profile for the 1st and 2nd discharge and 1st charge processes for varying reduction reaction rate constant of high-order polysulfide on the Li anode. For case (a) insignificant reduction reaction (b) intensive reduction reaction at anode side during charge state.

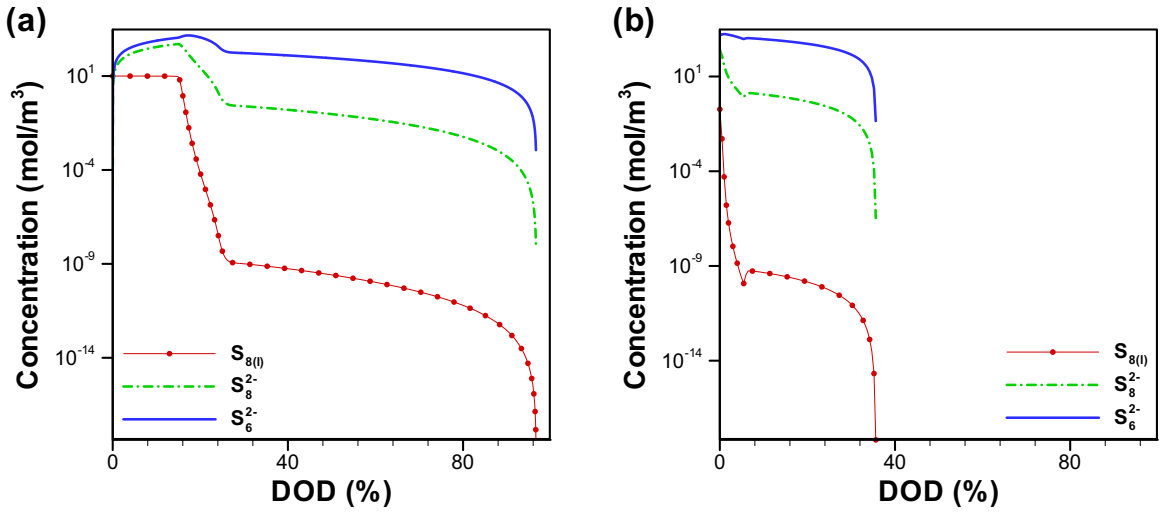

Fig. 7. Concentration of $S_{8(l)}$, S_8^{2} and S_6^{2-} in the cathode region for varying reduction reaction rate constant of high-order polysulfide on the Li anode during second discharge. For case (a) insignificant reduction reaction (b) intensive reduction reaction at the negative electrode during charging.

changes in intensity of the reduction reaction (Case A and D). Second discharge profiles were obtained for Case A and Case D as shown in Fig. 6. For Case A, the characteristic first and second plateaus are observed in the second discharge curve and the cell potential profile exactly corresponds to the first discharge profile (see Fig. 6 (a)). However, for Case D, the first potential plateau disappears in second discharge and the total specific capacity is also decreased (see Fig. 6(b)). As shown in the previous section, even if the cell was slightly overcharged for Case A, S_8^{2-} was fully recovered to $S_{8(l)}$, so that the reduction reaction ($S_{8(l)} \rightarrow S_8^{2-}$) happens in the first plateau region (0 ~ 30% DOD) (see Fig. 7 (a)). However, for Case-D, the S_8^{2-} concentration was constant during the overcharge process due to the polysulfides reduction reaction on the Li electrode and $S_{8(l)}$ was recovered at less than 30 mM. Therefore, in this case, the reduction reaction ($S_{8(l)} \rightarrow S_8^{2-}$) of higher order polysulfide ($S_{8(l)}$) disappears during the second discharge due to lack of reactant and this results in a lower specific capacity (see Fig. 7 (b)). This poor cycling performance has been reported for a Li/S cell consisting of a non-protected Li electrode and an electrolyte which has high solubility of polysulfides [1,31–33].

To investigate effects of polysulfide diffusivity and APL for the Li/S cell cycling performance, the simulations were carried out with different diffusivity values of polysulfides (Table 5) and various reduction reaction rate constants of polysulfides at the negative electrode. First, it was assumed that the electrolyte has high diffusivity and the reduction reaction at the negative electrode is fast. In this case, the specific capacity faded rapidly at 920 mAh/g after only five cycles (Fig. 8(a)). However, by limiting the reduction reaction of polysulfides at the negative electrode, we could predict better cycling performance (Fig. 8(b)). In this case, the specific capacity was maintained at over 1200 mA/g after the fifth cycle of operation. In addition, the rapid capacity fading could be alleviated by limiting the polysulfide mobility (see Fig. 8(c)). Even though high order polysulfides could still be reduced and consumed at the negative electrode during charging, the low mobility of polysulfides resulted in a low local concentration of polysulfides at the negative electrode, which suppressed the reduction reaction and improved the cycling performance. However, in this case, the overcharge problem was still evident due to the fast reaction at the negative electrode. Obviously, the simulation results showed that the best performance can be obtained with a slow reduction reaction of polysulfides at Li electrode and low polysulfide diffusivity (Fig. 8(d)). In this last case, the overcharge problem was hardly observed and the simulation showed 1300 mAh/g specific capacity after the fifth cycle.

Table 5
Diffusion coefficients of Li ion and Polysulfides. Diffusivity values are assumed based on viscosity of electrolyte mixture.

Species (i)	D_i (m^2/sec)	
	High Diffusion Case	Low Diffusion Case
Li^+	5×10^{-9}	1×10^{-10}
$S_{8(l)}$	1×10^{-8}	5×10^{-9}
S_8^{2-}	2×10^{-9}	1×10^{-10}
S_6^{2-}	4×10^{-9}	2×10^{-10}
S_4^{2-}	6×10^{-9}	3×10^{-10}
S_2^{2-}	8×10^{-9}	4×10^{-10}
S^{2-}	1×10^{-8}	5×10^{-9}

5. Conclusions

A modified model for the Li/S cell was proposed for analysis of the electrochemical characteristics of the Li/S cell. A reduction reaction of high-order polysulfides on the Li electrode was included in the model to investigate the polysulfide shuttling problem. Moreover, the existing kinetic model for the precipitation and dissolution was modified by adding an extra term for better numerical stability. The cell potential profiles were investigated considering the presence of solid sulfur phases $Li_2S_{(s)}$ and $Li_2S_{2(s)}$. By comparing the numerical results with experimental data obtained with different electrolytes, it is suggested that a mathematical model considering $S_{8(s)}$ and $Li_2S_{(s)}$ as the only possible solid species can predict the electrochemical performance of the Li/S cell most accurately. Also, the charging behavior of Li/S cells was modeled and analyzed with variations of the reaction rate constant of polysulfide reduction on the Li electrode and compared with experimental results for Li/S cells assembled with electrolytes containing $LiNO_3$ additive and ionic liquids. Numerical results reveal that the overcharge problem is significant with a higher reaction rate constant of polysulfide reduction on the Li electrode and cell charging is incomplete with electrolytes of high polysulfide solubility. These results agree well with experimental results of Li/S cells constructed with organic electrolytes in the absence of $LiNO_3$. Moreover, it is noted that the high voltage plateau was reduced markedly in the discharge process after incomplete charge because sulfur (S_8) could not be recovered

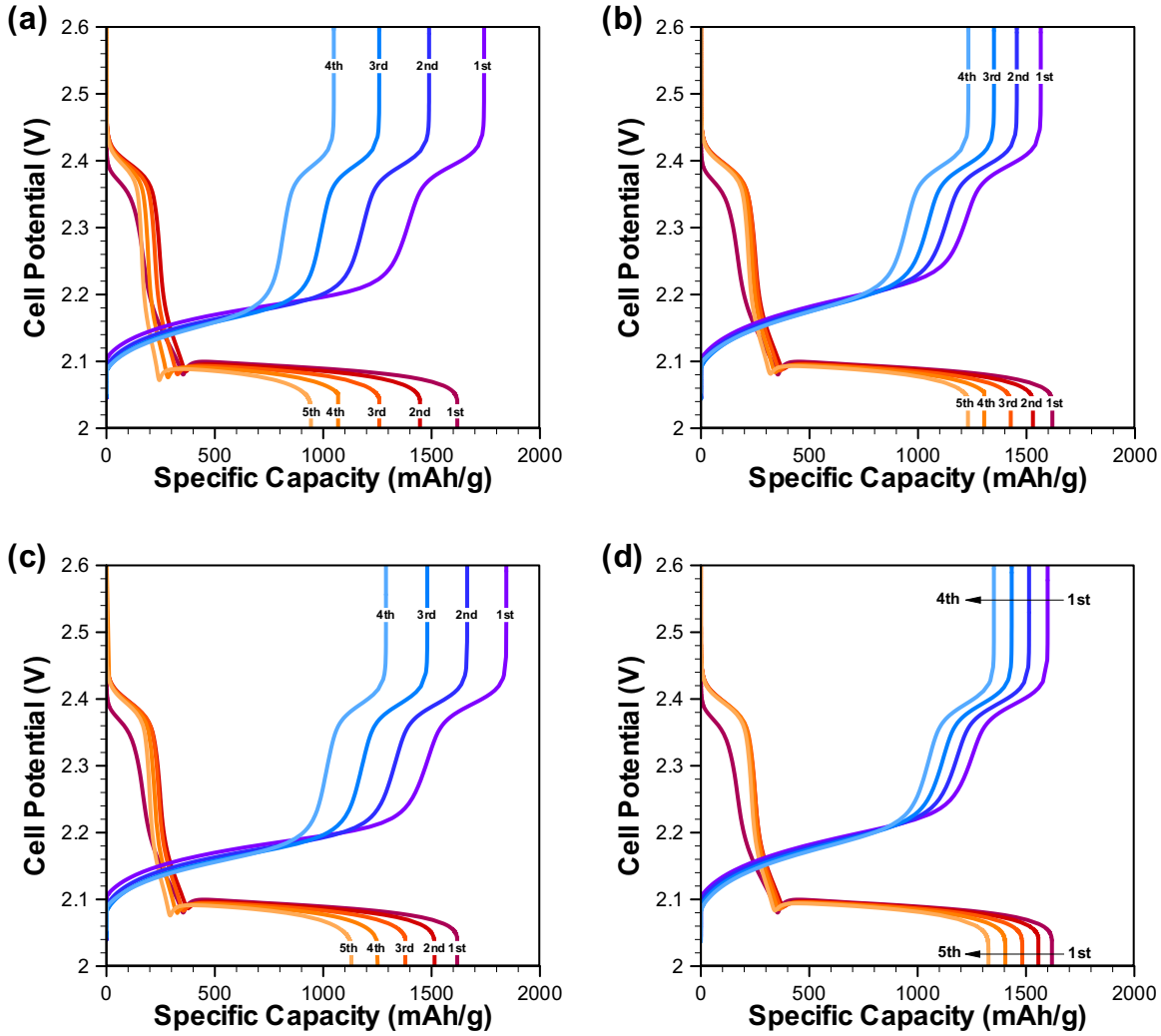

Fig. 8. Cycling performance of Li/S cell for various operation conditions. (a) high polysulfide diffusivity in electrolyte and high reduction reaction at the negative electrode (b) high polysulfide diffusivity and slow reduction reaction (c) low polysulfide diffusivity and fast reduction reaction (d) low polysulfide diffusivity and slow reduction reaction.

when the polysulfide shuttle problem is significant. Also, the cycling performance of the Li/S cell was investigated for various diffusivities of polysulfide and intensities of the reduction reaction at the negative electrode. Poor cycling performance was observed for high polysulfide diffusivity and intensive reduction reaction at the negative electrode which resulted in fast fading of specific capacity. However, notable improvement of cycling performance was achieved by limiting the polysulfide diffusivity and the reduction reaction rate at the negative electrode during charge.

Acknowledgment

This work was supported in part by the Washington State University Start-up grant.

References

[1] M.-K. Song, E.J. Cairns, Y. Zhang, Lithium/sulfur batteries with high specific energy: old challenges and new opportunities, Nanoscale 5 (2013) 2186–2204.
[2] P.G. Bruce, S.A. Freunberger, L.J. Hardwick, J.-M. Tarascon, Li-O2 and Li-S batteries with high energy storage, Nat Mater 11 (2012) 19–29.
[3] J. Nelson, S. Misra, Y. Yang, A. Jackson, Y. Liu, H. Wang, H. Dai, J.C. Andrews, Y. Cui, M.F. Toney, In operando X-ray diffraction and transmission X-ray microscopy of lithium sulfur batteries, Journal of the American Chemical Society 134 (2012) 6337–6343.
[4] M. Cuisinier, P.-E. Cabelguen, S. Evers, G. He, M. Kolbeck, A. Garsuch, T. Bolin, M. Balasubramanian, L.F. Nazar, Sulfur Speciation in Li-S Batteries Determined by Operando X-ray Absorption Spectroscopy, Journal of Physical Chemistry Letters 4 (2013) 3227–3232.
[5] A. Kawase, S. Shirai, Y. Yamoto, R. Arakawa, T. Takata, Electrochemical reactions of lithium-sulfur batteries: an analytical study using the organic conversion technique, Physical Chemistry Chemical Physics 16 (2014) 9344–9350.
[6] K. Kumaresan, Y. Mikhaylik, R.E. White, A mathematical model for a lithium-sulfur cell, Journal of the Electrochemical Society 155 (2008) A576–A582.
[7] M. Ghaznavi, P. Chen, Analysis of a mathematical model of lithium-sulfur cells Part III: Electrochemical reaction kinetics, transport properties and charging, Electrochimica Acta 137 (2014) 575–585.
[8] M. Ghaznavi, P. Chen, Sensitivity analysis of a mathematical model of lithium-sulfur cells part I: Applied discharge current and cathode conductivity, Journal of Power Sources 257 (2014) 394–401.
[9] M. Ghaznavi, P. Chen, Sensitivity analysis of a mathematical model of lithium-sulfur cells: Part II: Precipitation reaction kinetics and sulfur content, Journal of Power Sources 257 (2014) 402–411.
[10] Y.V. Mikhaylik, J.R. Akridge, Low temperature performance of Li/S batteries, Journal of the Electrochemical Society 150 (2003) A306–A311.
[11] E. Peled, Y. Sternberg, A. Gorenshtein, Y. Lavi, Lithium-sulfur battery – Evaluation of dioxolane-based electrolytes, Journal of the Electrochemical Society 136 (1989) 1621–1625.
[12] Y. Diao, K. Xie, S. Xiong, X. Hong, Shuttle phenomenon – The irreversible oxidation mechanism of sulfur active material in Li-S battery, Journal of Power Sources 235 (2013) 181–186.
[13] Y.V. Mikhaylik, J.R. Akridge, Polysulfide shuttle study in the Li/S battery system, Journal of the Electrochemical Society 151 (2004) A1969–A1976.
[14] A.F. Hofmann, D.N. Fronczek, W.G. Bessler, Mechanistic modeling of polysulfide shuttle and capacity loss in lithium-sulfur batteries, Journal of Power Sources 259 (2014) 300–310.
[15] Y.-J. Choi, Y.-D. Chung, C.-Y. Baek, K.-W. Kim, H.-J. Ahn, J.-H. Ahn, Effects of carbon coating on the electrochemical properties of sulfur cathode for lithium/sulfur cell, Journal of Power Sources 184 (2008) 548–552.

[16] H.S. Ryu, H.J. Ahn, K.W. Kim, J.H. Ahn, J.Y. Lee, Discharge process of Li/PVdF/S cells at room temperature, Journal of Power Sources 153 (2006) 360–364.
[17] S.S. Jeong, Y. Lim, Y.J. Choi, G.B. Cho, K.W. Kim, H.J. Ahn, K.K. Cho, Electrochemical properties of lithium sulfur cells using PEO polymer electrolytes prepared under three different mixing conditions, Journal of Power Sources 174 (2007) 745–750.
[18] S. Walus, C. Barchasz, J.-F. Colin, J.-F. Martin, E. Elkaim, J.-C. Lepretre, F. Alloin, New insight into the working mechanism of lithium-sulfur batteries: in situ and operando X-ray diffraction characterization, Chemical Communications 49 (2013) 7899–7901.
[19] J. Shim, K.A. Striebel, E.J. Cairns, The lithium/sulfur rechargeable cell – Effects of electrode composition and solvent on cell performance, Journal of the Electrochemical Society 149 (2002) A1321–A1325.
[20] K. Yoo, A. Deshpande, S. Banerjee, P. Dutta, Electrochemical model for ionic liquid electrolytes in lithium batteries, Electrochimica Acta 176 (2015) 301–310.
[21] K. Yoo, A.M. Dive, S. Kazemiabnavi, S. Banerjee, P. Dutta, Effects of operating temperature on the electrical performance of a Li-air battery operated with ionic liquid electrolyte, Electrochimica Acta 194 (2016) 317–329.
[22] L. Ji, M. Rao, H. Zheng, L. Zhang, Y. Li, W. Duan, J. Guo, E.J. Cairns, Y. Zhang, Graphene oxide as a sulfur immobilizer in high performance lithium/sulfur cells, Journal of the American Chemical Society 133 (2011) 18522–18525.
[23] M.K. Song, Y. Zhang, E.J. Cairns, Effects of cell construction parameters on the performance of lithium/sulfur cells, AIChE Journal 61 (2015) 2749–2756.
[24] J.H. Shin, E.J. Cairns, N-Methyl-(n-butyl)pyrrolidinium bis (trifluoromethanesulfonyl)imide-LiTFSI–poly(ethylene glycol) dimethyl ether mixture as a Li/S cell electrolyte, Journal of Power Sources 177 (2008) 537–545.
[25] J.H. Shin, E.J. Cairns, Characterization of N-Methyl-N-Butylpyrrolidinium Bis (trifluoromethanesulfonyl)imide-LiTFSI-Tetra(ethylene glycol) Dimethyl Ether Mixtures as a Li Metal Cell Electrolyte, Journal of The Electrochemical Society 155 (2008) A368–A373.
[26] A. Manthiram, Y. Fu, Y.-S. Su, Challenges and prospects of lithium-sulfur batteries, Accounts of Chemical Research 46 (2013) 1125–1134.
[27] Y.-X. Wang, S.-L. Chou, H.-K. Liu, S.-X. Dou, The electrochemical properties of high-capacity sulfur/reduced graphene oxide with different electrolyte systems, Journal of Power Sources 244 (2013) 240–245.
[28] S.S. Zhang, Role of LiNO3 in rechargeable lithium/sulfur battery, Electrochimica Acta 70 (2012) 344–348.
[29] G. Yang, S. Shi, J. Yang, Y. Ma, Insight into the role of Li2S2 in Li-S batteries: a first-principles study, Journal of Materials Chemistry A 3 (2015) 8865–8869.
[30] Y. Yang, G. Zheng, S. Misra, J. Nelson, M.F. Toney, Y. Gui, High-capacity micrometer-sized Li2S particles as cathode materials for advanced rechargeable lithium-ion batteries, Journal of the American Chemical Society 134 (2012) 15387–15394.
[31] J.-W. Park, K. Ueno, N. Tachikawa, K. Dokko, M. Watanabe, Ionic liquid electrolytes for lithium-sulfur batteries, Journal of Physical Chemistry C 117 (2013) 20531–20541.
[32] K. Dokko, N. Tachikawa, K. Yamauchi, M. Tsuchiya, A. Yamazaki, E. Takashima, J.-W. Park, K. Ueno, S. Seki, N. Serizawa, M. Watanabe, Solvate Ionic Liquid Electrolyte for Li-S Batteries, Journal of the Electrochemical Society 160 (2013) A1304–A1310.
[33] J.-W. Park, K. Yamauchi, E. Takashima, N. Tachikawa, K. Ueno, K. Dokko, M. Watanabe, Solvent effect of room temperature ionic liquids on electrochemical reactions in lithium-sulfur batteries, Journal of Physical Chemistry C 117 (2013) 4431–4440.